UCRL-CONF-202519

Spatial Analysis of Emissions Sources for HCCI Combustion at Low Loads Using a Multi-Zone Model

S.M. Aceves, D.L. Flowers, F. Espinosa-Loza, J. Martinez-Frias, J.E. Dec, M. Sjöberg, R.W. Dibble, R.P. Hessel

This article was submitted to
Society of Automotive Engineers Spring Fuels and Lubricants Meeting, Toulouse, France, June 8-10, 2004

U.S. Department of Energy
Lawrence Livermore National Laboratory

February 20, 2004

Spatial Analysis of Emissions Sources for HCCI Combustion at Low Loads Using a Multi-Zone Model

Salvador M. Aceves, Daniel L. Flowers, Francisco Espinosa-Loza, Joel Martinez-Frias
Lawrence Livermore National Laboratory

John E. Dec and Magnus Sjöberg
Sandia National Laboratories

Robert W. Dibble
University of California Berkeley

Randy P. Hessel
University of Wisconsin-Madison

ABSTRACT

We have conducted a detailed numerical analysis of HCCI engine operation at low loads to investigate the sources of HC and CO emissions and the associated combustion inefficiencies. Engine performance and emissions are evaluated as fueling is reduced from typical HCCI conditions, with an equivalence ratio ϕ = 0.26 to very low loads (ϕ = 0.04). Calculations are conducted using a segregated multi-zone methodology and a detailed chemical kinetic mechanism for iso-octane with 859 chemical species.

The computational results agree very well with recent experimental results. Pressure traces, heat release rates, burn duration, combustion efficiency and emissions of hydrocarbon, oxygenated hydrocarbon, and carbon monoxide are generally well predicted for the whole range of equivalence ratios. The computational model also shows where the pollutants originate within the combustion chamber, thereby explaining the changes in the HC and CO emissions as a function of equivalence ratio. The results of this paper contribute to the understanding of the high emission behavior of HCCI engines at low equivalence ratios and are important for characterizing this previously little explored, yet important range of operation.

INTRODUCTION

One of the outstanding issues associated with HCCI engine combustion is high carbon monoxide (CO) and hydrocarbon (HC) emissions. The levels of these emissions reported in the literature vary significantly between experiments [1-6], but they are typically found to be as high or higher than those of spark-ignition (SI) engines. The emission levels also vary significantly with operating condition, with most previous works showing an increase in both CO and HC at light loads and the percentage increase in CO emissions being substantially greater than that of HC. Controlling these emissions in-cylinder is particularly important at low loads since HCCI exhaust temperatures are very low, making the application of conventional oxidation catalysts challenging. Moreover, the low combustion efficiencies associated with these high emissions can result in a significant fuel-economy penalty, especially for a typical automotive urban driving cycle in which considerable time is spent at idle and low loads.

The source of these emissions has been found to be dependent on the fueling rate of the engine. For higher-load operating conditions both experimental and computational data have indicated that the main source of these emissions is the piston top ring-land crevice and near-wall regions. Christensen et al. [7] varied the geometry of the piston top-land crevice and concluded that it was the source of most of the HC emissions for their operating conditions (premixed HCCI using iso-octane at equivalence ratios of ϕ = 0.22 and higher). Similar results were found by Aceves et al. [8], using a multi-zone modeling approach to analyze the experimental results of Christensen et al. [7]. The modeling results in Aceves et al. [8] also indicated that a substantial portion of the CO was due to the crevices and boundary layers at these conditions.

For lower load operation, however, CO emissions can rise dramatically, reaching levels equivalent to 60% of the fuel carbon at fueling rates typical of idle in diesel engines (ϕ = 0.1 to 0.12) [4,5,9,10]. Hydrocarbon and oxygenated hydrocarbon (OHC) levels also increase, but at a slower rate than CO [4,9]. OHCs are toxic pollutants consisting of formaldehyde and other compounds [4,5]. Corresponding to these high levels of CO, HC, and OHC emissions, combustion efficiencies can fall below 60%. Single-zone modeling studies [9,10] and combined experimental and modeling results [4], have shown that these high emissions at low loads result from incomplete combustion throughout the bulk gas. This occurs

at a slower rate than CO [4,9]. OHCs are toxic pollutants consisting of formaldehyde and other compounds [4,5]. Corresponding to these high levels of CO, HC, and OHC emissions, combustion efficiencies can fall below 60%. Single-zone modeling studies [9,10] and combined experimental and modeling results [4], have shown that these high emissions at low loads result from incomplete combustion throughout the bulk gas. This occurs because combustion temperatures become so low at these very dilute conditions (*i.e.*, low equivalence ratios) that the reactions are not complete before they are quenched by expansion. The CO-to-CO_2 reactions are particularly sensitive to the combustion temperature. For operation at 1200 rpm with combustion phasing at TDC and using iso-octane as the fuel, a minimum peak temperature on the order of 1500 K is required to complete CO oxidation [4,6]. A more recent detailed investigation has shown that this peak temperature is independent of both fuel type and combustion phasing [11], although it does vary somewhat with engine speed [6].

In order to better understand the changes in HCCI emissions and combustion efficiency with changes in fueling rate, Dec and Sjöberg [4] recently conducted a comprehensive study involving both detailed experiments and single-zone chemical-kinetic modeling. In this study, the fueling rate was systematically varied from ϕ = 0.26 down to ϕ = 0.04 in steps of 0.02. These equivalence ratios cover the range from typical HCCI operating conditions to a well-below-idle fueling that is the near the limit for determining the heat release from the cylinder pressure trace. The data showed that at higher fueling rates, CO, HC, and OHC emissions were low and not strongly affected by changes in ϕ. However, as fueling was reduced, CO emissions begin to rise. The increase was gradual at first, then as ϕ dropped below 0.2 the CO level began to rise rapidly, and HC and OHC levels also increased.

In the current paper, we conduct a detailed analysis of the experimental results presented in Ref. [4]. The analysis is based on a segregated multi-zone methodology that makes it possible to solve the fluid mechanics separate from the chemical kinetics, thereby greatly reducing the computational time while providing accurate results. This paper complements the experimental and numerical results of [4] by providing detailed spatially resolved information. The main objective of this work is to provide an understanding of how the sources of CO and HC emissions transition from crevices and/or near-wall regions to the bulk-gas as fueling is reduced. The paper also demonstrates the applicability of the multi-zone model at very low loads, which represents a previously unexplored range of HCCI engine modeling.

The following two sections give brief descriptions of the experimental work and the numerical methodology used in this paper. The reader is referred to [4,12] for more detailed descriptions. Iso-octane was used as the fuel for both the experiment and the model to facilitate comparison.

EXPERIMENTAL WORK

The engine used for this investigation is derived from a Cummins B-series production diesel engine, which is a typical medium-duty diesel engine with a displacement of 0.98 liters/cylinder. This engine was converted into a balanced single-cylinder HCCI research engine through several modifications, as described in Ref. [4]. The engine is equipped with a custom HCCI piston as shown in Fig. 1. This modified-pancake combustion chamber design was chosen because it provided a large squish clearance and a minimum top ring-land crevice volume that amounts to only 1.4% of the top dead center (TDC) volume for the 17.63:1 compression-ratio piston used in this study. The engine specifications and operating conditions are listed in Table 1.

Table 1. Engine and Injector Specifications

Displacement (single-cylinder)	0.981 liters
Bore	102 mm
Stroke	120 mm
Connecting Rod Length	192 mm
Geometric Compression Ratio	17.63:1
IVO	717° ‡
IVC	205° ‡
EVO	480° ‡
EVC	8° ‡
Fuel	Iso-Octane
Intake pressure	120 kPa
Intake temperature	140°C
Engine speed	1200 rpm
Equivalence ratio	0.04-0.26

‡ 0° CA is taken to be TDC intake.

For this study, all fueling was accomplished using a fully premixed fueling system in which liquid fuel is supplied to an electrically heated vaporizer chamber by means of a GDI fuel injector. The vaporizing chamber consists of a cavity machined into a block of copper that is electrically heated to 150°C. The fuel vaporizes as the spray impinges on the floor of this chamber whose temperature is well above the 98-99°C atmospheric boiling point of iso-octane, which was the fuel used for this investigation. The vaporized fuel was introduced into the intake air line upstream of the intake surge tank to insure adequate mixing. To provide precise control over the equivalence ratio supplied, the fuel was metered by means of a positive-displacement flow meter, and the intake air was metered with a sonic nozzle.

Intake air was supplied by an air compressor, dehumidified to a dew point of 4°C by a refrigerated dryer, and electrically heated to the desired intake temperature. The engine was coupled to a 125-hp dynamometer that could either motor the engine or absorb load to maintain a constant engine speed.

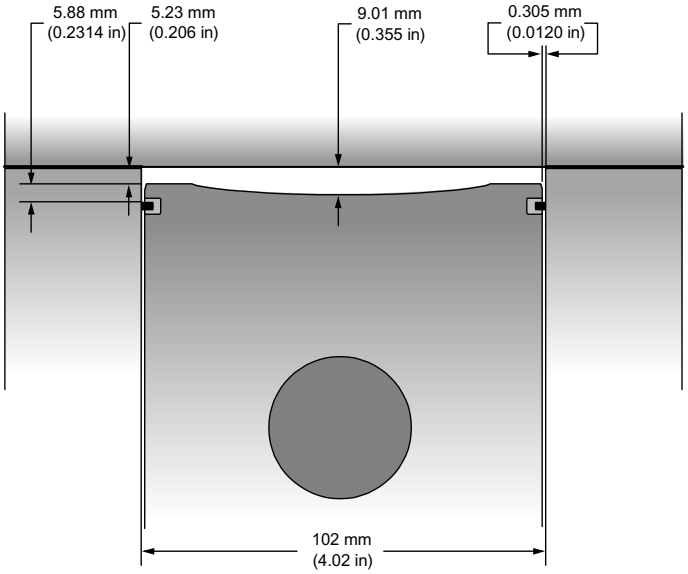

Figure 1. Schematic of the HCCI piston geometry and combustion chamber dimensions at TDC.

For each operating condition, the cylinder pressure, fuel-injection pressure, and intake and exhaust pressures and temperatures were recorded, in addition to the emissions data. All experimental results for pressure traces, heat release rates and the pressure-indicated thermal efficiency are 100-cycle averages.

Exhaust emissions data were acquired after the engine operation had stabilized (typically after 5 minutes of operation), with the sample being drawn from the exhaust plenum using a heated sample line. For all conditions, the levels of CO, CO_2, HC, NO_X and O_2 were measured using standard exhaust-gas analysis equipment [4]. Smoke measurements were made with an automated smoke meter. However, for all conditions reported here, smoke levels were too low to be detected, so they are not presented.

The engine was instrumented with a thermocouple embedded in the firedeck 2.5 mm beneath the surface. For each equivalence ratio, these thermocouple measurements were recorded. An apparent firedeck surface temperature was computed by linear extrapolation, assuming that the back surface of the firedeck was at the cooling water temperature of 100°C. The results are shown in Fig. 2. These temperatures are necessary for conducting a detailed analysis of the experimental data. Cylinder-liner and piston temperatures were not measured. Instead, they were set according to previous experience [12]. The cylinder liner temperature was assumed equal to the fire deck temperature, and the piston temperature was assumed to be 50 K hotter than the firedeck.

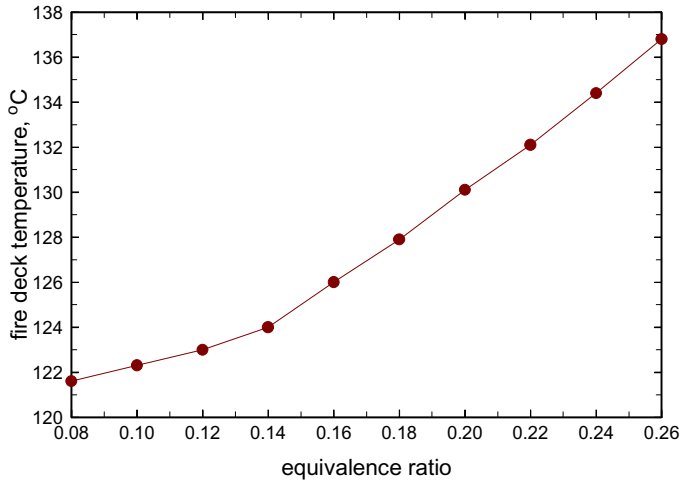

Figure 2. Fire deck temperature as a function of equivalence ratio.

ANALYSIS

Figure 3 illustrates the overall sequence of calculations required for the multi-zone method. The procedure is started by making a KIVA3V run considering motored (no ignition) conditions. The resulting geometric temperature distribution, shown in Figure 3(a), is then converted into a temperature mass distribution. The temperature mass distribution gives the fraction of the total mass in the cylinder that has a certain temperature. Figure 3(b) shows a typical temperature mass distribution at TDC and a cumulative mass distribution, which indicates the fraction of the mass that is colder than a specified temperature T. The mass within the cylinder is then assigned to temperature zones. The number of zones is selected, as well as a mass distribution within the zones. For this work, the mass was distributed among 40 zones. Previous research has shown that 40 zones are necessary to properly resolve the small regions of the cylinder where HC and CO are typically produced [13]. The computational expense of using 40 zones has been considerably reduced by the development of a segregated solver [14]. A 40-zone run with a detailed iso-octane mechanism takes 1 day on a single processor 2 GHz PC running Linux.

The temperature-weighted mass distributions are calculated from KIVA3V for multiple crank angles during the compression stroke. These temperature distributions are used for calculating zone temperature histories. Figure 3(c) shows a temperature history for 10 zones. The temperature histories are the geometry-specific information that is passed from KIVA3V to the chemical kinetics code (HCT; Hydrodynamics, Chemistry and Transport [15]) to yield results that satisfactorily consider the effects of both fluid mechanics and chemical kinetics. HCT is run in multi-zone mode starting at intake valve

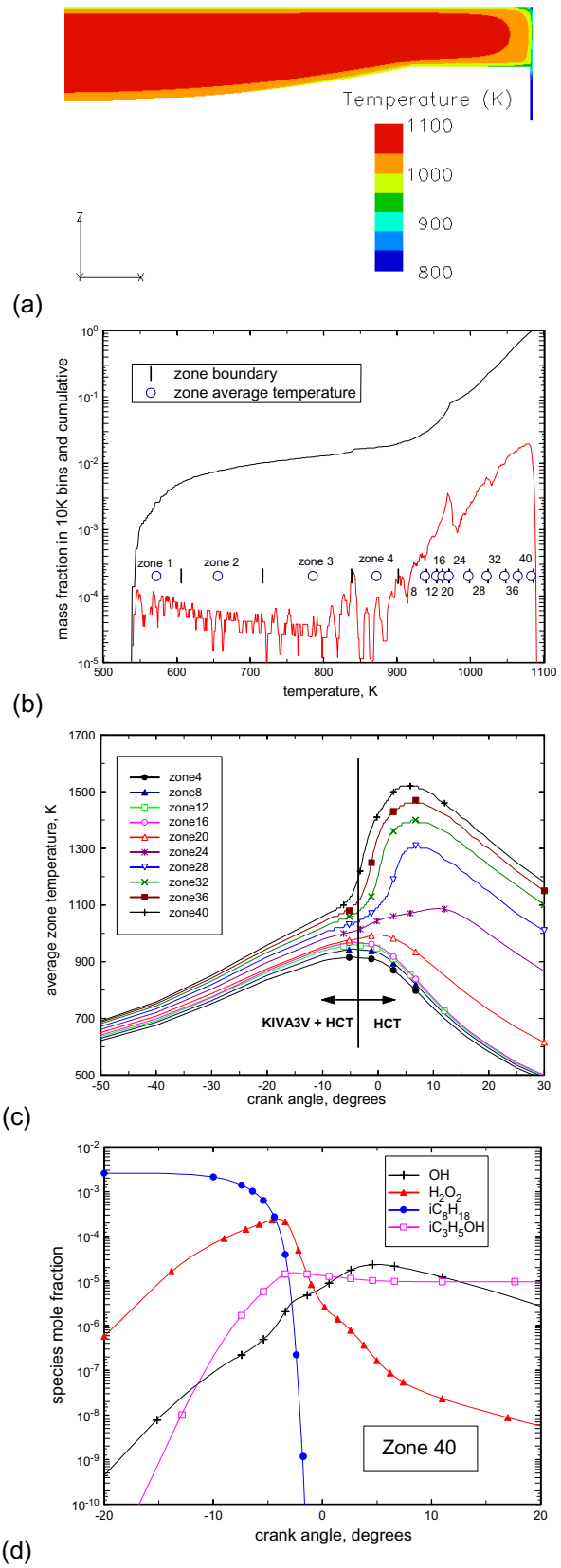

Figure 3. The main steps in the sequential multi-zone analysis of HCCI combustion. (a) Calculation of temperatures inside the cylinder from KIVA3V. (b) Calculation of mass distribution as a function of temperature. (c) Calculation of temperature histories for the zones. (d) Detailed chemical kinetics HCT run with temperature histories determined from KIVA3V.

closing and continuing until the end of the expansion stroke. The zone temperatures in HCT follow the temperature histories obtained from KIVA3V during the compression stroke, until the point of ignition (defined as the crank angle at which the cumulative energy release reaches 5% of the total available chemical energy). After ignition, the KIVA3V temperature histories are abandoned and pressure and zone temperatures are determined from basic thermodynamic equations [14] and the Woschni heat transfer correlation [16]. The multi-zone HCT calculates all combustion parameters, including pressure, burn duration, heat release, combustion efficiency, exhaust emissions, radical concentration (Figure 3(d)) and all the details about the chemical kinetics during HCCI combustion. The model as applied here does not consider the effect of mixing between zones.

Three grids were generated for the cylinder geometry. These are a low-resolution grid (13,000 elements), a baseline grid (51,000 elements), and a high-resolution grid (197,000 elements). The grids were tested against experimental data for both motored cases and firing cases, and little difference was observed between the three grids. Due to the favorable agreement, the baseline grid was used for all the results presented. Figure 4 shows the axisymmetric baseline grid. The chemical kinetics code (HCT) uses a detailed chemical kinetics model for iso-octane that includes 859 species and 3606 chemical reactions [17].

Pressure traces are matched by adjusting the temperature at intake valve closing (IVC) to obtain the appropriate ignition timing. Pressure at IVC may also be slightly adjusted to obtain a good match for the peak cylinder pressure. The same initial pressure and temperature were used for all the zones. Composition at IVC was determined by taking into account the effect of residual gases, although the residual gas fraction is small in all cases. No other parameters are adjusted in the model, and all the default parameters are used in KIVA3V for wall heat transfer, turbulence, etc. The chemical kinetic mechanism is used in its original form with no modifications.

RESULTS

Figure 5 shows a comparison between the experimental and the numerical pressure traces for the 12 cases being analyzed ($0.04 \leq \phi \leq 0.26$ in steps of 0.02). The figure shows experimental results with solid lines and numerical results with dashed lines. The figure shows a very good agreement in all cases. Agreement is in general comparable to the results obtained in previous multi-zone studies [12,14].

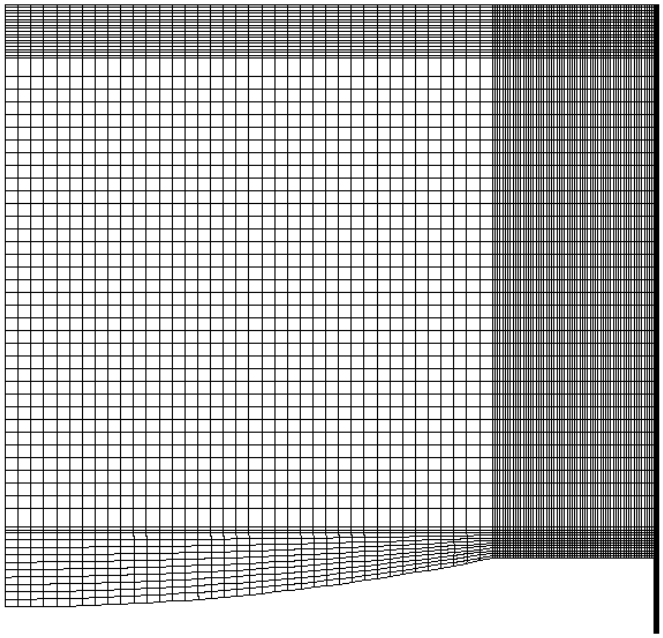

Figure 4. View of axisymmetric baseline grid at 60 degrees before TDC. The grid has 51000 elements. The grid is too dense to show in the crevices.

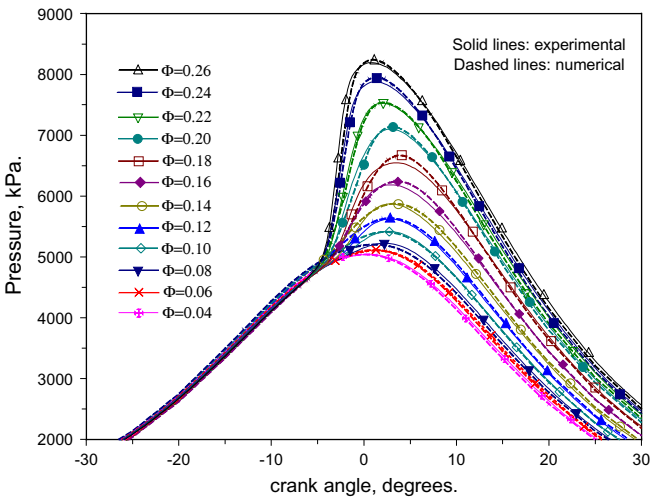

Figure 5. Comparison between experimental and numerical pressure traces for the 12 cases being analyzed. The figure shows experimental results with solid lines and numerical results with dashed lines.

Figures 6 and 7 show a comparison between experimental and numerical apparent heat release rates for the 12 cases considered. The apparent heat release rate was calculated with a published procedure [18]. The results are divided into two figures to improve readability. The figures show experimental results with solid lines and numerical results with dashed lines. Figure 6 shows the results for $\phi \geq 0.18$ and Figure 7 shows the results for $\phi \leq 0.18$. Figure 6 also shows a few results for $\phi \leq 0.18$ to facilitate comparison between the two figures. The figures show good agreement between numerical and experimental heat release rates, although the model tends to underestimate slightly the peak heat release rate. This is especially true at the lowest equivalence ratios (Figure 7). Agreement in other combustion parameters, such as burn duration, is very good. Some of the disagreement in heat release rate may be due to the uncertainty in wall temperature. A sensitivity analysis is necessary to determine how the wall temperature may affect heat release rate.

Figure 8 shows a comparison between experimental and numerical results for engine emissions as a function of equivalence ratio. In Figure 8, the emissions are given as the percentage of total fuel carbon in each of the exhaust

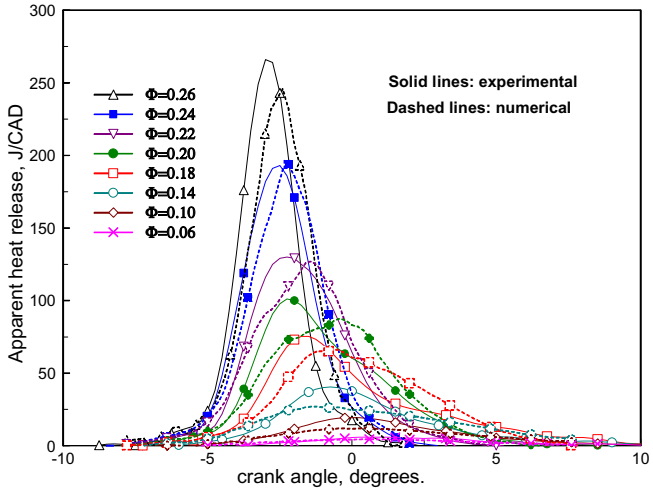

Figure 6. Comparison between numerical and experimental apparent heat release rates for all the cases with $\phi \geq 0.18$ and three cases with $\phi < 0.18$. The figure shows experimental results with solid lines and numerical results with dashed lines.

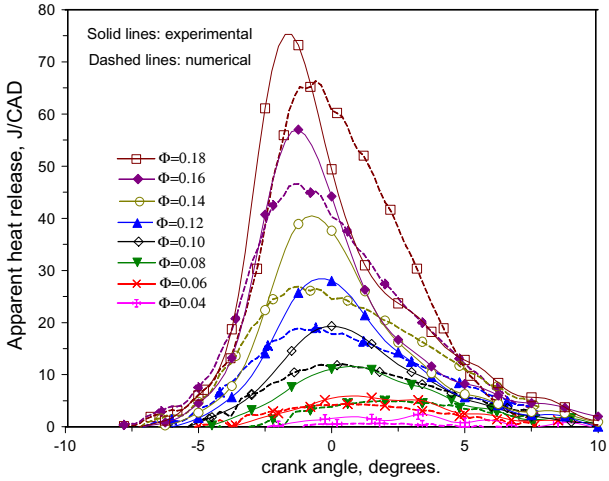

Figure 7. Comparison between numerical and experimental apparent heat release rates for the 8 cases considered with low equivalence ratios ($\phi \leq 0.18$). The figures show experimental results with solid lines and numerical results with dashed lines.

species (CO_2, CO, OHC and HC) in order to remove changes due solely to the quantity of fuel supplied (i.e. the emissions are normalized by the amount of fuel). The figure shows experimental results with solid lines and numerical results with dashed lines. Figure 8 shows that experimentally measured CO emissions rise dramatically as fueling is reduced, reaching a maximum value of 63% of the total fuel carbon. Carbon monoxide emissions then drop, as the equivalence ratio is further reduced to 0.04. Figure 8 also shows that even at the highest fuel load (ϕ = 0.26), 2.9% of the fuel carbon remains as unburned HC. Moreover, the shape of the HC curve in Figure 8 indicates that the HC emissions are approaching an asymptote with the HC levels changing only slightly from ϕ = 0.22 to 0.26. As ϕ is reduced below 0.22, the HC emissions increase, slowly at first and then more rapidly. OHC emissions follow a similar trend, increasing monotonically as the equivalence ratio is reduced.

Figure 8 shows that there is good agreement between experimental and numerical results for engine emissions as a function of equivalence ratio. The numerical results (dashed lines) slightly overpredict CO_2 and HC emissions while underpredicting CO and OHC emissions. The model does a good job at predicting emissions at high fueling rates, where most HC and CO emissions originate in the crevices. Predictions are also good at mid and low fueling rates, where emissions originate both at the crevices and in the bulk gases. The model predicts the non-monotonic behavior of CO emissions as the equivalence ratio is reduced to very low levels (below idle fueling, ϕ < 0.1). This non-monotonic behavior can be explained in terms of the progress of the reactions that produce CO from the fuel and the reactions that consume the CO that was previously formed. This topic is further discussed later in this paper.

As illustrated in Figure 8, the numerical predictions for CO and CO_2 emissions would be very accurate if the equivalence ratio for the numerical results were shifted up in equivalence ratio by 0.02. This is similar to the results obtained by Dec and Sjöberg [4], where it was found that the results from a single zone model would predict experimental CO emissions well if offset in equivalence ratio by ϕ=0.04. In our case, we believe the ϕ=0.02 offset in CO and CO_2 emissions exists because the multi-zone model, as implemented here, does not take into account mixing between zones. Recent research [19] has indicated that there is enough time during the expansion stroke for unburned fuel to migrate from the crevices and boundary layer into the hot core of the cylinder, where it can react and produce additional CO and CO_2. Future work with an integrated KIVA3V-HCT model will allow us to explore these details with accuracy.

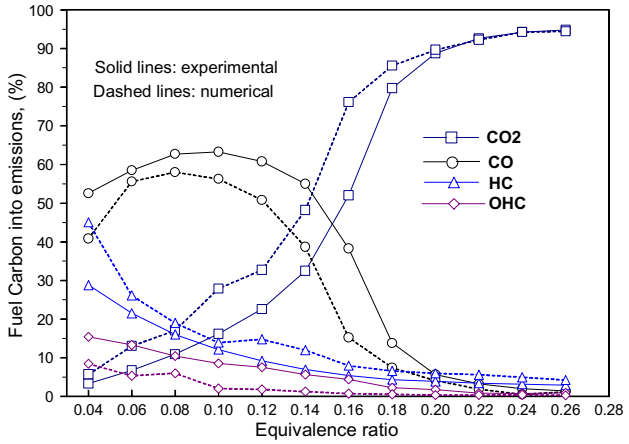

Figure 8. Comparison between experimental and numerical results for engine emissions as a function of equivalence ratio. Emissions are given as the percentage of total fuel carbon in each of the exhaust species (CO_2, CO, OHC and HC). The figure shows experimental results with solid lines and numerical results with dashed lines.

Figure 9 shows a comparison between experimental and numerical results for combustion efficiency. As can be seen, the combustion efficiency drops slowly as the equivalence ratio is reduced between 0.26 and 0.20. Then, as the equivalence ratio is reduced below 0.18, the combustion efficiency drops faster, in an approximately linear fashion. For fueling rates corresponding to idle (ϕ = 0.1 to 0.12), the combustion efficiency has fallen to only about 55% (experiment) or 59% (numerical). At ϕ = 0.04, the combustion efficiency is only 32%.

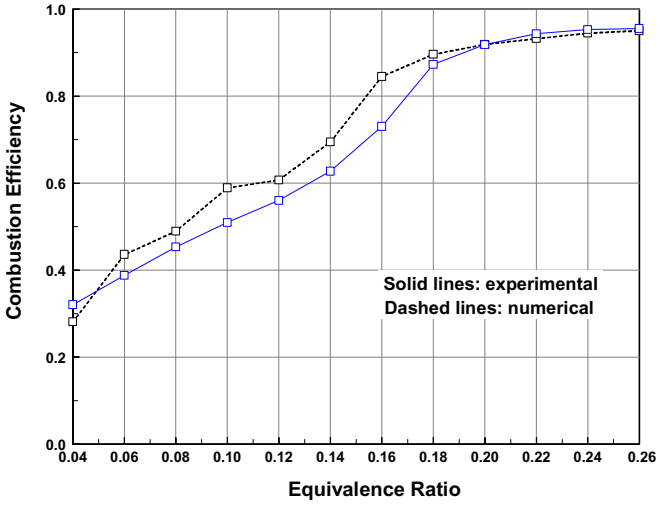

Figure 9. Comparison between experimental and numerical results for combustion efficiency as a function of equivalence ratio. The figure shows experimental results with solid lines and numerical results with dashed lines.

Figure 9 shows that there is generally good agreement between numerical results (dashed line) and experimental results (solid line). The numerical results are close to the experimental results for the whole range, although combustion efficiency is slightly overpredicted for a wide part of the range ($0.18 \geq \phi \geq 0.06$). As with the emissions data in Figure 8, the agreement would be much closer if the numerical results were offset by 0.02 equivalence-ratio units.

Figure 10 shows the spatial distribution of HC- and CO-producing regions in the cylinder. These results help explain the cause of the changes in HC and CO emission levels (Figure 8) and combustion efficiency (Figure 9) as a function of ϕ. Figure 10 shows, for four representative equivalence ratios, the distribution of the mass that burns to completion, the mass that reacts partially into CO, the mass that reacts partially into intermediate hydrocarbons and fuel, and the mass that does not react at all and remains as unburned fuel. Figure 10 shows results for ϕ = 0.26, 0.16, 0.10 and 0.04.

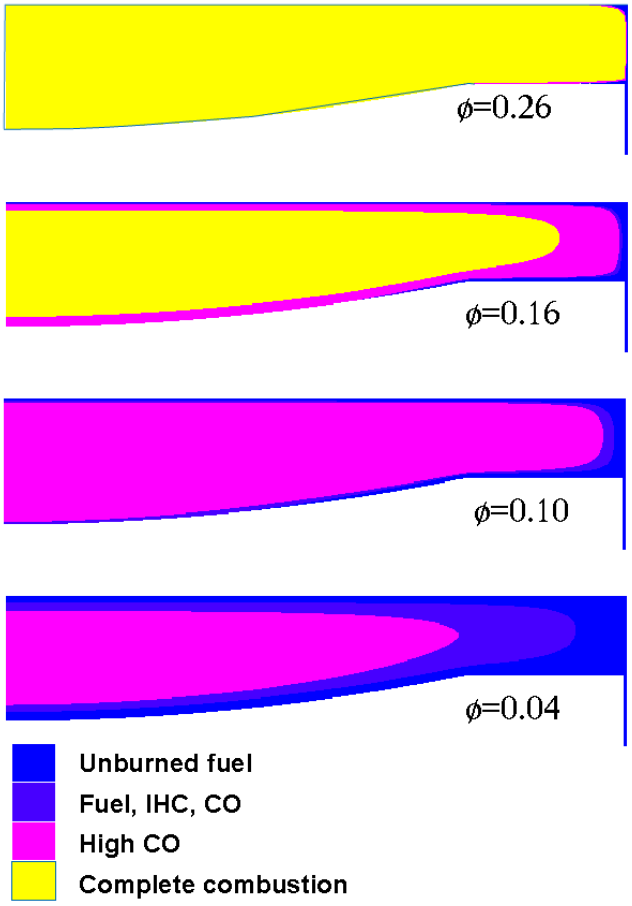

Figure 10. Geometrical distribution of the mass that burns to completion, the mass that reacts partially into CO, the mass that reacts partly into intermediate hydrocarbons and fuel, and the mass that does not react at all and remains as unburned fuel. The geometrical distribution is shown at 6°BTDC for four values of equivalence ratio ϕ = 0.26, 0.16, 0.10 and 0.04.

The mass distribution for ϕ=0.26 in Figure 10 shows results that correspond closely with those previously studied for typical HCCI operating conditions [8,12]. Under these relatively high load conditions, burnt-gas temperatures are sufficiently high throughout the core gases for reactions to go to completion, forming CO_2. Hydrocarbon and CO emissions result from crevices and boundary layer, which are too cold to react to completion. Crevices have a high surface-to-volume ratio that keeps temperatures too low for combustion, and the crevice contains 1.4% of the TDC volume, so on a volume basis alone it accounts for about half of the 2.9% of fuel carbon that becomes HC emissions. In addition, crevice temperatures are well below bulk-gas temperatures, causing the mass-fraction in the crevice to exceed its TDC volume-fraction.

The ϕ = 0.16 results in Figure 10 show the spatial distribution near the onset in the rapid rise in CO emissions noted in Figure 8. At this lower equivalence ratio, the conditions start diverging from those typically found in HCCI engines at high load. In this case, the core temperature is still high enough to yield complete combustion. However, there is a broad boundary layer where the temperatures are not hot enough for complete combustion. In the boundary layer, combustion stops early in the expansion stroke, resulting in a high concentration of CO. As the gases cool down during the expansion stroke, the concentration of OH radicals drops rapidly, stopping the conversion of CO into CO_2 [11,13].

As fueling is further reduced to idle-like conditions, CO emissions are near their maximum, and the ϕ = 0.10 results in Figure 10 are representative of the mass distribution. The core temperatures are now too low for reactions to go to completion, and most of the gases in the cylinder react partially to form CO. Figure 8 indicates that at this fueling rate, over 60% of the carbon atoms in the fuel are going into CO. Cold gases in the crevices do not react and produce unburned fuel emissions. A narrow boundary layer produces intermediate hydrocarbons, including oxygenated hydrocarbons.

The case ϕ=0.04 is the lowest equivalence ratio considered. At this equivalence ratio, combustion temperatures are extremely low (the maximum temperature of the burned gases is 1130 K, only 30 K above the maximum temperature during a motored cycle). At these conditions, only the central core reacts into CO, while there is a wide boundary layer region that burns partially into intermediate hydrocarbons. This explains why the CO emissions drop and the HC emissions increase as the equivalence ratio is reduced below ϕ=0.10. At ϕ=0.04, unburned fuel still originates in the crevices and in a thin boundary layer.

Figures 11, 12 and 13 are shown to illustrate in more detail the information presented in Figure 10. These figures show the spatial distributions of the fraction of carbon atoms in the fuel that remains as unreacted iso-octane (Figure 11), the fraction of carbon atoms that reacts partially into intermediate hydrocarbons and OHC

(Figure 12), and the fraction of carbon atoms that reacts partially into CO (Figure 13).

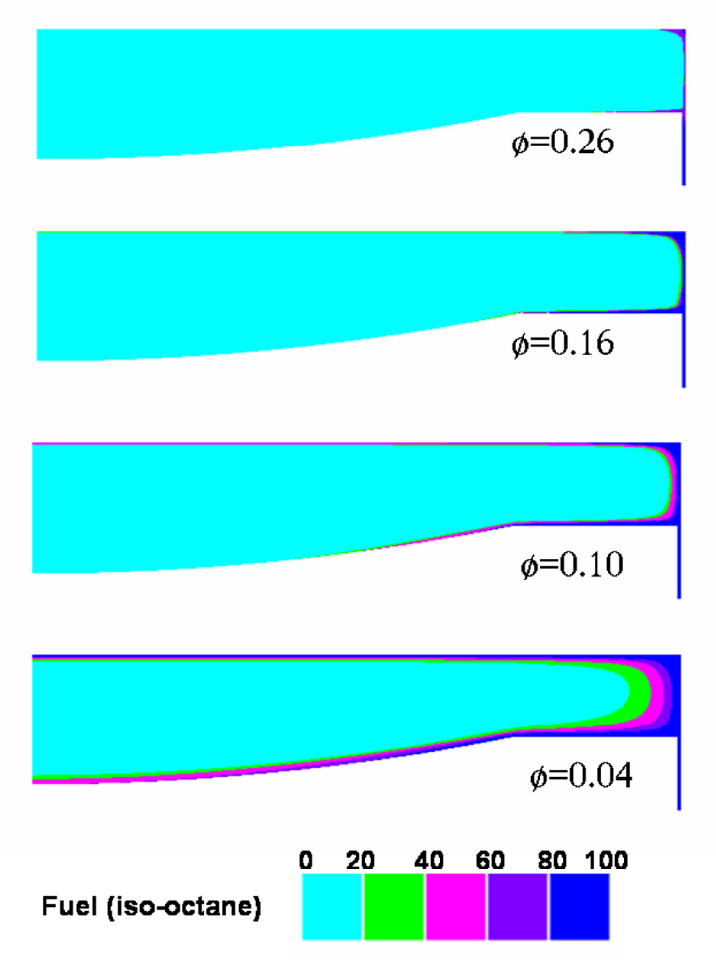

Figure 11. Geometrical distribution of the fraction of carbon atoms in the fuel that do not react and remain as fuel. The geometrical distribution is shown at 6°BTDC for four values of equivalence ratio ϕ = 0.26, 0.16, 0.10 and 0.04. The scale shows the percentage of fuel carbon atoms that remain as fuel.

Figure 11 shows that the sources of unreacted fuel are the crevices and boundary layers. Even as the equivalence ratio is reduced to 0.04, the core reacts enough to decompose most of the fuel into intermediate hydrocarbon, OHC, CO and CO_2. At the bottom of the crevices, the temperature is too low for any reaction to occur and 100% of the carbon remains as unburned fuel for all equivalence ratios.

The distribution of intermediate hydrocarbons shown in Figure 12 indicates that at the high equivalence ratio (ϕ=0.26) most intermediate hydrocarbons originate from the crevices and wall region. As the equivalence ratio is reduced, the region with high intermediate hydrocarbon migrates from the crevice and wall region into a broad boundary layer region (ϕ=0.04). The distribution of intermediate hydrocarbon is non monotonic. The concentration of intermediate hydrocarbon is low at the core (where fuel reacts to CO and CO_2) and low in the crevices (where fuel remains unreacted), reaching a maximum in the middle of the distribution, as illustrated by the dark regions in Figure 12. The fraction of carbon going to intermediate hydrocarbon reaches a maximum of approximately 35%.

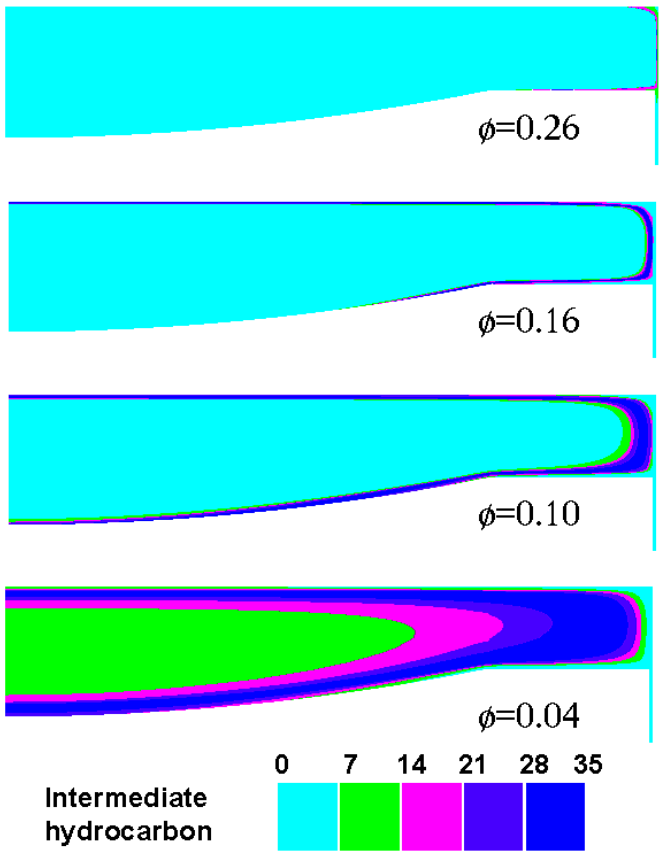

Figure 12. Geometrical distribution of the fraction of carbon atoms in the fuel that react partially into intermediate hydrocarbons and OHC. The geometrical distribution is shown at 6°BTDC for four values of equivalence ratio ϕ = 0.26, 0.16, 0.10 and 0.04. The scale shows the percentage of fuel carbon atoms that react partially into intermediate hydrocarbons.

The fraction of carbon atoms going into carbon monoxide is shown in Figure 13. The CO distribution also migrates from the wall region at the high equivalence ratio (ϕ=0.26) to the core at the low equivalence ratio (ϕ=0.04). The CO distribution is also non-monotonic, except for the lowest equivalence ratio (ϕ=0.04) where the maximum CO fraction is obtained in the core. The maximum fraction of carbon atoms going into CO is very high (over 70%).

Taken together, Figures 11-13 illustrate well how the thermal distribution in the combustion chamber influences how far the combustion in each region progresses along the path: fuel $\Rightarrow$ intermediate HC $\Rightarrow$ OHC $\Rightarrow$ CO $\Rightarrow$ CO_2. Clearly, the combustion progress for each fluid parcel is dependent on both the global

equivalence ratio and the local temperature before the onset of combustion.

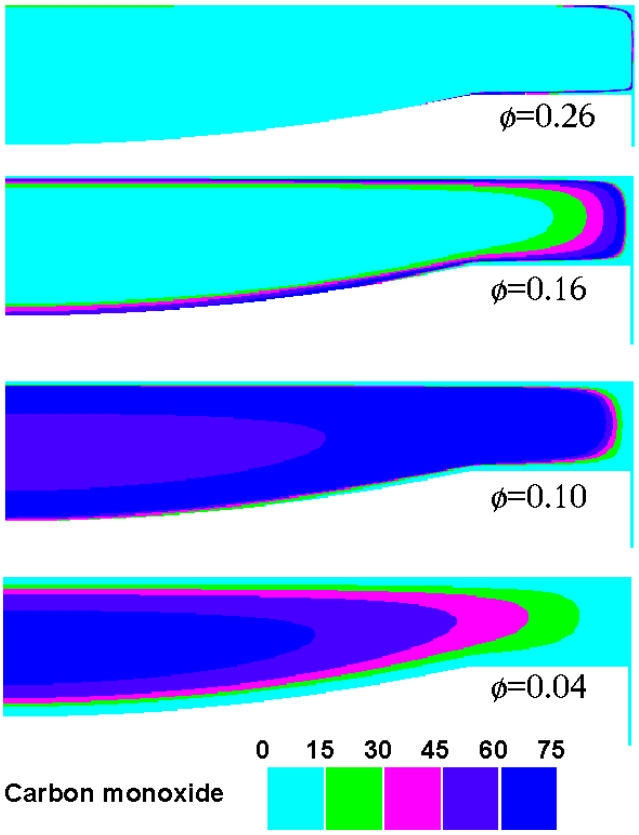

Figure 13. Geometrical distribution of the fraction of carbon atoms in the fuel that react partially into carbon monoxide. The geometrical distribution is shown at 6°BTDC for four values of equivalence ratio ϕ = 0.26, 0.16, 0.10 and 0.04. The scale shows the percentage of fuel carbon atoms that react partially into carbon monoxide.

Figure 14 shows a comparison between experimental and numerical results for CO, total HC (HC plus OHC), and combustion efficiency. The figure shows the ratio of numerical to experimental values as a function of equivalence ratio. A value of one in Figure 14 indicates a perfect agreement between experimental and numerical results. The figure shows good agreement in most parameters. Combustion efficiency has near perfect agreement for all high load cases ($\phi \geq 0.18$). All previous multi-zone HCCI analyses fall in this high load regime where HC and CO emissions originate mainly in the crevices. Under these conditions, the model tends to underestimate CO emissions because the model does not consider diffusion between zones. Unburned HC from the crevices can potentially diffuse into the hot core gases in the cylinder, reacting partially to form CO emissions. This mechanism is also partly responsible for the overprediction of HC emissions at high load. Recent work [19] has demonstrated that including diffusion between zones in the model considerably improves prediction of HC and CO emissions in this high load operating range.

For low equivalence ratios (ϕ < 0.18), conditions diverge from those found in previous HCCI engine analyses, which were conducted at higher loads. Under these low load conditions, bulk gases become the dominant source of CO and HC emissions, and diffusion of HC from the crevices to the core is no longer a major source of CO. This explains the fact that prediction of CO emissions improves considerably as the equivalence ratio is reduced below 0.16. Figure 14 also shows that total HC emissions are well predicted at low equivalence ratios, even though OHC are underpredicted and non-oxygenated HC emissions are overpredicted (Figure 8).

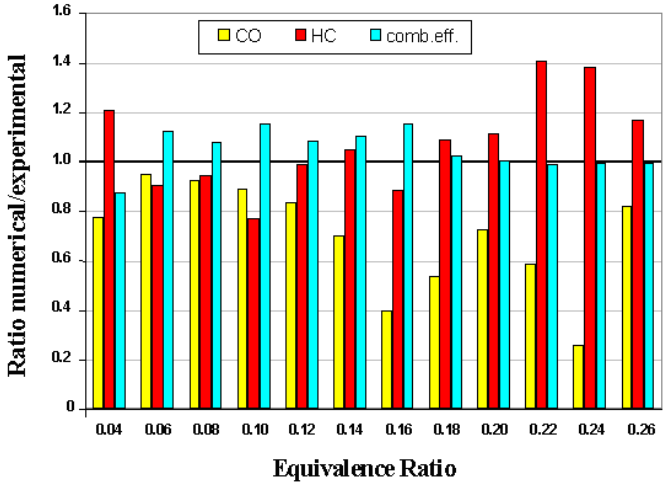

Figure 14. Ratio of numerical to experimental values for CO emissions, total HC (HC plus OHC) emissions, and combustion efficiency as a function of equivalence ratio. A value of one in the figure indicates a perfect agreement between experimental and numerical results.

SUMMARY AND CONCLUSIONS

This paper has shown a detailed numerical analysis of a recent experimental study of an HCCI engine over a wide range of fueling rates, from near-knocking conditions to loads well below idle. The experiments were conducted in a single-cylinder research engine with a displacement of 0.98 liters and a compression ratio of 17.63. The engine was equipped with a custom piston providing an open combustion chamber and a minimal ring-land crevice. Iso-octane was used as the fuel for all experiments to facilitate comparison with the model. Twelve fueling rates were examined, with ϕ varying from 0.26 to 0.04 in steps of 0.02 (idle fueling corresponds to ϕ = 0.10 - 0.12). The analysis is based on a segregated multi-zone methodology that makes it possible to solve the fluid mechanics separate from the chemical kinetics, thereby greatly reducing the computational time while providing accurate results. This multidimensional analysis complements the experimental and single-zone computational results of Ref. [4], by showing how the

spatial location of CO and HC formation shifts from crevices and/or near-wall regions to the bulk-gas as fueling is reduced. The paper also demonstrates the applicability of the multi-zone model at very low loads, which represents a previously unexplored yet important range of HCCI engine modeling. The study produced the following results:

1. The model predicts with good accuracy pressure traces and heat release rates for the 12 cases being analyzed. Agreement is similar to the results obtained in previous publications [8,12]. Other combustion parameters such as burn duration and combustion efficiency are also well predicted.
2. The experimental results show that the engine produces substantial CO emissions at values of ϕ corresponding to idle-like fueling rates (63% of all carbon in the fuel goes into CO at ϕ=0.10). As the equivalence ratio is reduced further the emissions of CO drop and the emissions of HC and OHC increase. The model does a very good job of predicting the trends in the CO, HC, and OHC emissions as a function of equivalence ratio. The absolute values are also in reasonable agreement, with the exception that the model results are offset about 0.02 equivalence-ratio units lower than the experiment.
3. The multi-zone model has the capability of showing where in the combustion chamber the different pollutants originate.
   - At high equivalence ratios (ϕ=0.26), the results correspond closely with those previously studied for typical HCCI operating conditions, with hydrocarbon and CO emissions originating at crevices and boundary layer, which are too cold to react to completion.
   - As the equivalence ratio is reduced to ϕ=0.16, the conditions start diverging from those typically found in HCCI engines at high load. In this case, there is a broad boundary layer zone where the temperature is not hot enough for complete combustion in the available time. In the boundary layer, combustion stops early in the expansion stroke, resulting in a high concentration of CO.
   - The mass distribution for ϕ=0.10 shows that the temperature is low enough that even the core is too cold to react to completion, and most of the gases in the cylinder react partially to form CO. This condition corresponds to the maximum level of CO emissions observed in the experiment.
   - Finally, at ϕ=0.04 combustion temperatures are extremely low, so that only the central core reacts into CO, while there is a wide boundary layer region that burns partially into intermediate hydrocarbons. This explains why the CO emissions drop and the HC emissions increase as the equivalence ratio is reduced below ϕ=0.10.

ACKNOWLEDGMENTS

This project is funded by DOE, Office of FreedomCAR and Vehicle Technologies, Steve Goguen and Gurpreet Singh, program managers. Work performed under the auspices of the U.S. Department of Energy by University of California, Lawrence Livermore National Laboratory under Contract W-7405-ENG-48.

REFERENCES

1. Aoyama, T., Yoshiaki, H., Mizuta, J., and Sato, Y., “An Experimental Study on Premixed-Charge Compression Ignition Gasoline Engine,” SAE Paper 960081, 1996.
2. Christensen, M., Johansson, B., and Einewall, P., “Homogeneous Charge Compression Ignition (HCCI) Using Iso-octane, Ethanol, Natural Gas – A Comparison with Spark Ignition,” SAE Paper 972874, 1997.
3. Gray, A. W. and Ryan-III, T. W., “Homogeneous Charge Compression Ignition (HCCI) of Diesel Fuel,” SAE Paper 971676, 1997.
4. Dec, J.E., and Sjöberg, M. “A Parametric Study of HCCI Combustion – the Sources of Emissions at Low Loads and the Effects of GDI Fuel Injection,” SAE Paper 2003-01-0752, 2003.
5. Kaiser, E. W., Yang, J., Culp, T., Xu, N., and Maricq, M. M., “HCCI Engine-Out Emissions – Does Flame Propagation Occur in HCCI,” *Int. J. Engine Research*, Vol. 3, pp. 185-195, 2002.
6. Sjöberg, M. and Dec, J. E., “Combined Effects of Fuel-Type and Engine Speed on Intake Temperature Requirements and Completeness of Bulk-Gas Reactions in an HCCI Engine,” SAE Paper 2003-01-3173, 2003.
7. Christensen, M., Johansson, B., and Hultqvist, A., “The Effect of Piston Topland Geometry on Emissions of Unburned Hydrocarbons from a Homogeneous Charge Compression Ignition (HCCI) Engine,” SAE Paper 2001-01-1893, 2001.
8. Aceves, S.M., Flowers, D.L., Espinosa-Loza, F., Martinez-Frias, J., Dibble, R.W., Christensen, M., Johansson, B., Hessel, R.P., “Piston-Liner Crevice Geometry Effect on HCCI Combustion by Multi-Zone Analysis,” SAE Paper 2002-01-2869, 2002.
9. Dec, J. E., “A Computational Study of the Effects of Low Fuel Loading and EGR on Heat Release Rates and Combustion Limits in HCCI Engines,” SAE Paper 2002-01-1309, 2002.
10. Yamasaki, Y. and Iida, N., “Numerical Analysis of Auto Ignition and Combustion of n-Butane and Air Mixture in the Homogeneous Charge Compression Ignition Engine by Using Elementary Reactions,” 5th COMODIA 2001, July 1-4, Nagoya, Japan, pp. 417-425, 2001.
11. Sjöberg, M. and Dec, J. E., “An Investigation into Lowest Acceptable Combustion Temperatures for Hydrocarbon Fuels in HCCI Engines,” Submitted to

the 30th International Symposium on Combustion, Chicago, IL, July 25-30, 2004.
12. Aceves, S. M., Flowers, D. L., Martinez-Frias, M., Dibble, R., Wright, J. F., Akinyemi, W. C., and Hessel, R. P., "A Sequential Fluid-Mechanic Chemical-Kinetic Model of Propane HCCI Combustion," SAE Paper 2001-01-1027, 2001.
13. Flowers, D. L., Aceves, S. M., Martinez-Frias, J., and Dibble, R. W., Prediction of Carbon Monoxide and Hydrocarbon Emissions in Iso-Octane HCCI Engine Combustion Using Multi-Zone Simulations," *Proc. Combust. Inst.*, Vol. 29, 2002.
14. Aceves, S.M., Martinez-Frias, J., Flowers, D.L., Smith, Dibble, R.W., Wright, J.F., and Hessel, R.P., "A Decoupled Model of Detailed Fluid Mechanics Followed by Detailed Chemical Kinetics for Prediction of Iso-Octane HCCI Combustion," SAE Paper 2001-01-3612, 2001.
15. Lund, C. M., "HCT - A General Computer Program for Calculating Time-Dependent Phenomena Involving One-Dimensional Hydrodynamics, Transport, and Detailed Chemical Kinetics," Lawrence Livermore National Laboratory report UCRL-52504, 1978.
16. Woschni, G., "Universally Applicable Equation for the Instantaneous Heat Transfer Coefficient in the Internal Combustion Engine," SAE Paper 670931, 1967.
17. Curran, H. J., Gaffuri, P., Pitz, W. J., and Westbrook, C. K., "A Comprehensive Modeling Study of Iso-Octane Oxidation," Combustion and Flame, Vol. 129, pp. 253-280, 2002.
18. Heywood, J. B., Internal Combustion Engine Fundamentals, McGraw-Hill, Inc., New York, NY, 1988.
19. Flowers, D. L., Aceves, S. M., Martinez-Frias, J., Hessel, R.P., and Dibble, R. W., "Effects of Mixing on Hydrocarbon and Carbon Monoxide Emissions, Predictions for Isooctane HCCI Engine Combustion Using a Multi-Zone Detailed Kinetics Solver," SAE Paper 2003-01-1821, 2003.